Stratum-by-stratum projection of light response attributes by retinal bipolar cells of *Ambystoma*

Ji-Jie Pang, Fan Gao and Samuel M. Wu

Cullen Eye Institute, Baylor College of Medicine, Houston, TX 77030, USA

The visual system processes light images by projecting various representations of the visual world to segregated regions in the brain through parallel channels. Retinal bipolar cells constitute the first parallel channels that carry different light response attributes to different parts of the inner plexiform layer (IPL). Here we present a systematic study on detailed axonal morphology and light response characteristics of over 200 bipolar cells in dark-adapted salamander retinal slices by the whole-cell voltage clamp and Lucifer yellow fluorescence (with a confocal microscope) techniques. Four major groups of bipolar cells were identified according to the patterns of axon terminal ramification in the IPL: 36% were narrowly monostratified (whose axon terminals ramified in one of the 10 strata of the IPL), 27% were broadly monostratified, 19% were multistratified, and 18% bore pyramidally branching axons. By analysing the bipolar cells with narrowly monostratified axon terminals in each of the 10 strata of the IPL, we found that several key light response attributes are highly correlated with the strata in which the cells' axon terminals ramify. The 10 IPL strata appear to be the basic building blocks for attributes of light-evoked signal outputs in all bipolar cells, and several general stratum-by-stratum rules were identified by analysing the broadly monostratified, multistratified and pyramidally branching cells. These rules not only uncover mechanisms by which third-order retinal cells integrate and compute bipolar cell signals, but also shed considerable light on how bipolar cells in other vertebrates process visual information and how physiological signals may shape the morphology and projection of output synapses of visual neurones during development.

(Received 26 February 2004; accepted after revision 10 May 2004; first published online 14 May 2004)
Corresponding author S. M. Wu: Cullen Eye Institute, Baylor College of Medicine, One Baylor Plaza, NC-205, Houston, TX 77030, USA. Email: swu@bcm.tmc.edu

In addition to topologically mapping two-dimensional images of the outside world onto the two-dimensional array of retinal photoreceptors in each eye, the visual system projects different attributes of light signals through parallel channels to segregated regions in the brain (Enroth-Cugell & Robson, 1966; Hubel & Wiesel, 1977; Hubel & Livingstone, 1987). The first segregated projection region in the visual system is the inner plexiform layer (IPL) of the retina, in which output synapses of ON bipolar cells ramify at the proximal half (sublamina B) and those of the OFF bipolar cells ramify at the distal half of the IPL (sublamina A) (Famiglietti. & Kolb, 1976; Nelson *et al.* 1978). In mammalian retinas, anatomical studies have shown that rod bipolar cells send their axon terminals to the proximal regions of the IPL whereas cone bipolar cells send axons to more distal regions (Boycott & Wassle, 1991, 1999; Euler & Wassle, 1995; Roska & Werblin, 2001), but physiological characterization of light response attributes in these cells is still fragmentary. Moreover, it has been suggested that the mammalian retina contains more than a dozen types of retinal ganglion cells, each with dendrites ramifying at different strata in the IPL and each carrying a unique representation of the visual world (Roska & Werblin, 2001; Roska & Werblin, 2003). It is not clear, however, how retinal bipolar cells project various attributes of visual signals to different IPL strata for the ganglion cells to generate stratum-specific light responses. A systematic stratum-by-stratum analysis of the bipolar cell light responses is needed.

By comparing light responses and the cell morphology, a recent study has shown that bipolar cells in the salamander retina can be divided into 12 types, each exhibiting a unique set of light response attributes and a different pattern of axon terminal morphology in the IPL (Wu *et al.* 2000). However, this 12-type classification scheme may be incomplete because of the limited sample size

 DOI: 10.1113/jphysiol.2004.063503

and imprecise visualization of axonal processes by the conventional light microscope. Additionally, since this scheme only includes narrowly monostratified bipolar cells in five of the 10 strata of the IPL, it is difficult to determine complete stratum-by-stratum rules for the entire IPL. In this study, we investigated over 200 bipolar cells in living tiger salamander retinal slices and correlated their light response characteristics with more precise axon terminal morphology by studying Lucifer yellow fluorescence images with a confocal microscope. In addition to the 12 types of bipolar cells reported in the previous study, we found many more morphologically distinguishable types of bipolar cells, including narrowly monostratified cells in all 10 IPL strata. Moreover, we found that the axon terminal morphology of these cells correlates in an orderly fashion with several key light response attributes, which leads to the identification of stratum-by-stratum rules for narrowly monostratified cells and general rules for all bipolar cells. These rules describe how various attributes of light-evoked signals are projected to different regions of the IPL (where synapses with third-order retinal cells are made), and how parallel signalling pathways are organized in the visual system.

Methods

Larval tiger salamanders (*Ambystoma tigrinum*) purchased from Charles D. Sullivan, Co. (Nashville, TN, USA) and KON's Scientific Co. Inc. (Germantown, WI, USA) were used in this study. All animals were handled in accordance with the policies on treatment of laboratory animals of Baylor College of medicine and the National Institutes of Health.

Before each experiment, salamanders were anaesthetized in MS222 until the animal gave no visible response to touch or water vibration. The animals were then quickly decapitated and the eyes were enucleated. The procedures of dissection, retinal slicing and recording were described in previous publications (Werblin, 1978; Wu, 1987*b*). Dissection and recording were done under infrared illumination with a dual-unit Fine-R-Scope and the Nitemare infrared scopes BE Meyers, Redmond, WA, USA. Oxygenated Ringer solution was introduced continuously to the superfusion chamber, and the control Ringer solution contained 108 mM NaCl, 2.5 mM KCl, 1.2 mM $MgCl_2$, 2 mM $CaCl_2$ and 5 mM Hepes (adjusted at pH 7.7). All chemicals were dissolved in control Ringer solution. A photostimulator was used to deliver light spots (of diameter 600–1200 μm) to the retina via the epi-illuminator of the microscope. The intensity of unattenuated ($\log I = 0$) 500 nm light was 2.05×10^7 photons $\mu m^{-2}\,s^{-1}$. Since we delivered an un-collimated stimulus light beam through an objective lens with large numerical aperture (Zeiss 40×/0.75 water), the incident light entered the retinal slice in many directions, and thus the effect of photoreceptor self-screening was minor (Field & Rieke, 2002). The peak amplitude of light-evoked current responses was plotted against light stimulus intensity, and data points were fitted by the Hill equation:

$$R/R_{\max} = I^N/(I^N + \sigma^N)$$
$$= 0.5[1 + \tanh 1.15N(\log I - \log \sigma)]$$

where R is the current response amplitude, $R_{\max}$ is the maximum response amplitude, σ is the light intensity that elicits a half-maximal response, N is the Hill coefficient, tanh is the hyperbolic tangent function and log is the logarithmic function of base 10. In this article, we used the R–log I plot for our analysis (the right-hand term of the above equation), and for such plots the light intensity span (dynamic range, DR: range of intensity that elicits responses between 5 and 95% of $R_{\max}$) of a cell equals $2.56/N$ (Thibos & Werblin, 1978).

Voltage-clamp recordings were made with an Axopatch 200A amplifier (Axon Instruments, Union City, CA, USA) connected to a DigiData 1200 interface and pCLAMP 6.1 software. Patch electrodes of 5 MΩ tip resistance (when filled with an internal solution containing 118 mM caesium methanesulphonate, 12 mM CsCl, 5 mM EGTA, 0.5 mM $CaCl_2$, 4 mM ATP, 0.3 mM GTP, 10 mM Tris, 0.8 mM Lucifer yellow (Sigma, St Louis, MO, USA), and when adjusted to pH 7.2 with CsOH) were made with Narishige or Sutter patch electrode pullers. The chloride equilibrium potential (E_{Cl}) with this internal solution was about −60 mV. The equilibrium potential of cation current was determined by the reversal potential of glutamate-induced current in morphologically identified bipolar cells in Ringer solution containing 2 mM Co^{2+} (Wu & Maple, 1998). Light-elicited photoreceptor and amacrine cell inputs to bipolar cells were studied by recording the light-evoked cation and chloride currents, ΔI_C and ΔI_{Cl}, at holding potentials E_{Cl} and E_C, respectively. Estimates of the liquid junction potential at the tip of the patch electrode prior to seal formation varied from −9.2 to −9.6 mV. For simplicity, we corrected all holding potentials by 10 mV. Spontaneous and light-evoked current responses were analysed by in-house software and SigmaPlot (Jandel, San Rafael, CA, USA). The average unitary sEPSCs (I_1) in HBCs were analysed by the variance/mean method described by Katz & Miledi (1972). In this analysis, we approximated individual sEPSCs as 'shot' effects because the rising phase

of sEPSCs is very fast (≤ 1 ms), and at least some events appeared to have single-exponential decay. This leads to $I_1 =$ (variance of the cation current noise)/(2 × difference mean current in darkness and in bright light). If the decay time courses of individual sEPSC events are multiple exponential, our estimate will be off by a factor between 1 and 2 (Katz & Miledi, 1972).

Three-dimensional cell morphology was visualized in living retinal slices (250–300 μm in thickness) through the use of Lucifer yellow fluorescence with a confocal microscope (Zeiss 510). Images were acquired by using a × 40 water immersion objective (n.a. = 0.75), the 458 nm excitation line of an argon laser, and a long pass 505 nm emission filter. Consecutive optical sections were superimposed to form a single image using Zeiss LSM PC software, and these compressed image stacks were further processed in Adobe Photoshop 6.0 to improve the contrast. Since signal intensity values were typically enhanced during processing to improve the visibility of smaller processes, the cell bodies and larger processes of some cells appear saturated due to their larger volume of fluorophore. Although the background images of the retinal slices were acquired simultaneously with the fluorescent cells, they were imaged using transmitted light. The level at which dendritic processes stratified in the IPL was characterized by the distance from the processes to the distal margin of the IPL. We selected cells in the bipolar cell layers with somas situated beneath the surface of the slice and they usually had relatively intact processes (assessed by rotation of the stacked images).

Results

Distribution of axon terminal stratification patterns of bipolar cells

Figure 1*A* shows the stacked confocal fluorescence image of a bipolar cell in a living retinal slice (*Aa*), a sketch of the same cell on a schematic background of a retina with the IPL divided into 10 strata (*Ab*), and the light-evoked current responses to a 0.5-s light step at various holding potentials (*Ac*). Typical bipolar cell features (labelled in Fig. 1*Ab*) include a cell body (CB) centred in the distal half of the inner nuclear layer (INL), a Landolt club extending into the outer nuclear layer, dendrites branching in the outer plexiform layer (OPL), and an axon (A) with terminal processes (AT) ramifying laterally within the IPL. The bipolar cell in Fig. 1*A* is an example of what we termed a bipolar cell with pyramidally branching axons (cells with axonal processes terminated at a narrow level within the IPL, with an initial branching at more distal levels of the IPL). By using this protocol, we studied a total of 202 bipolar cells; 73 (36%) were 'narrowly monostratified' (with axon terminals ramifying in one of the 10 strata of the IPL), 53 (27%) were 'broadly monostratified' (axon terminals ramifying in 2–4 contiguous strata), 39 (19%) were 'multistratified' (dendrites ramifying in two or more non-contiguous strata), and 37 (18%) had pyramidally branching axons. The distribution of bipolar cell axon terminal stratification levels in the IPL is given in Fig. 1*B*. Each vertical column represents a bipolar cell and the short vertical bars in individual strata indicate the presence of axonal processes in that stratum. Asterisks indicate the initial branching points and the small dots indicate the branch passage. Cells were arranged in the order of the number of their axonal strata (narrowly monostratified cells first, within which cells were arranged in the order of their axonal stratum 1–10). In this sample of 202 bipolar cells, about 2/3 (64%) were monostratified, more than half of which were narrowly ramified in a single stratum.

In each of the bipolar cells listed in Fig. 1*B*, we measured light-evoked current responses at various holding potentials. Depolarizing bipolar cells (DBCs, or ON-centre cells) were identified as cells with *inward* excitatory light-evoked cation current (ΔI_C) recorded at E_{Cl} (near −60 mV, see Methods), and hyperpolarizing bipolar cells (HBCs, or OFF-centre cells) were identified as cells with *outward* ΔI_C. In this paper, we shall use DBCs and HBCs instead of ON-centre and OFF-centre cells, and leave the terms ON and OFF for the cells' responses to the onset and offset of the light step. DBCs and HBCs were labelled as ○ and ●, respectively, below each cell column in Fig. 1*B*.

Stratum-by-stratum rules for DBC/HBC, excitatory and inhibitory light-evoked currents, ON/OFF responses, rod/cone dominance and spontaneous excitatory currents (sEPSCs) in narrowly monostratified bipolar cells

We first analysed ΔI_C and ΔI_{Cl} of narrowly monostratified bipolar cells. Since these cells have axon terminals ramifying in only one IPL stratum, it is easier to determine the stratum-by-stratum rules of the bipolar cell light responses. Figure 2 shows ΔI_C and ΔI_{Cl} (lower panel) of 10 (marked as cells 1–10, corresponding to the stratum each cell ramifies, one from each horizontal row of cell nos 1–73 in Fig. 1*B*) narrowly monostratified cells whose axon terminals ramified in each of the 10 strata of the IPL. The upper panel shows stacked confocal fluorescence images of narrowly monostratified bipolar cells in living retinal slices (extended portions of wider

axon terminals were cut off in order to save space). The thickness of axon terminals (in the dimension parallel with the photoreceptor axes) of the majority (65–75%) of the narrowly monostratified cells was about 1/10 of the thickness of the IPL, whereas about 15% were slightly wider than 1/10 of the IPL and the rest were somewhat thinner than 1/10 of the IPL. Most axon terminals appeared slightly wavy in the IPL because the contours of the ganglion cell and amacrine cell somas lining the IPL were not completely straight. Additionally, since the contours of ganglion and amacrine cell somas in different depths of the retinal slice were not distributed like a perfect lattice, the *stacked* image of axon terminals sometimes had the '∞' appearance.

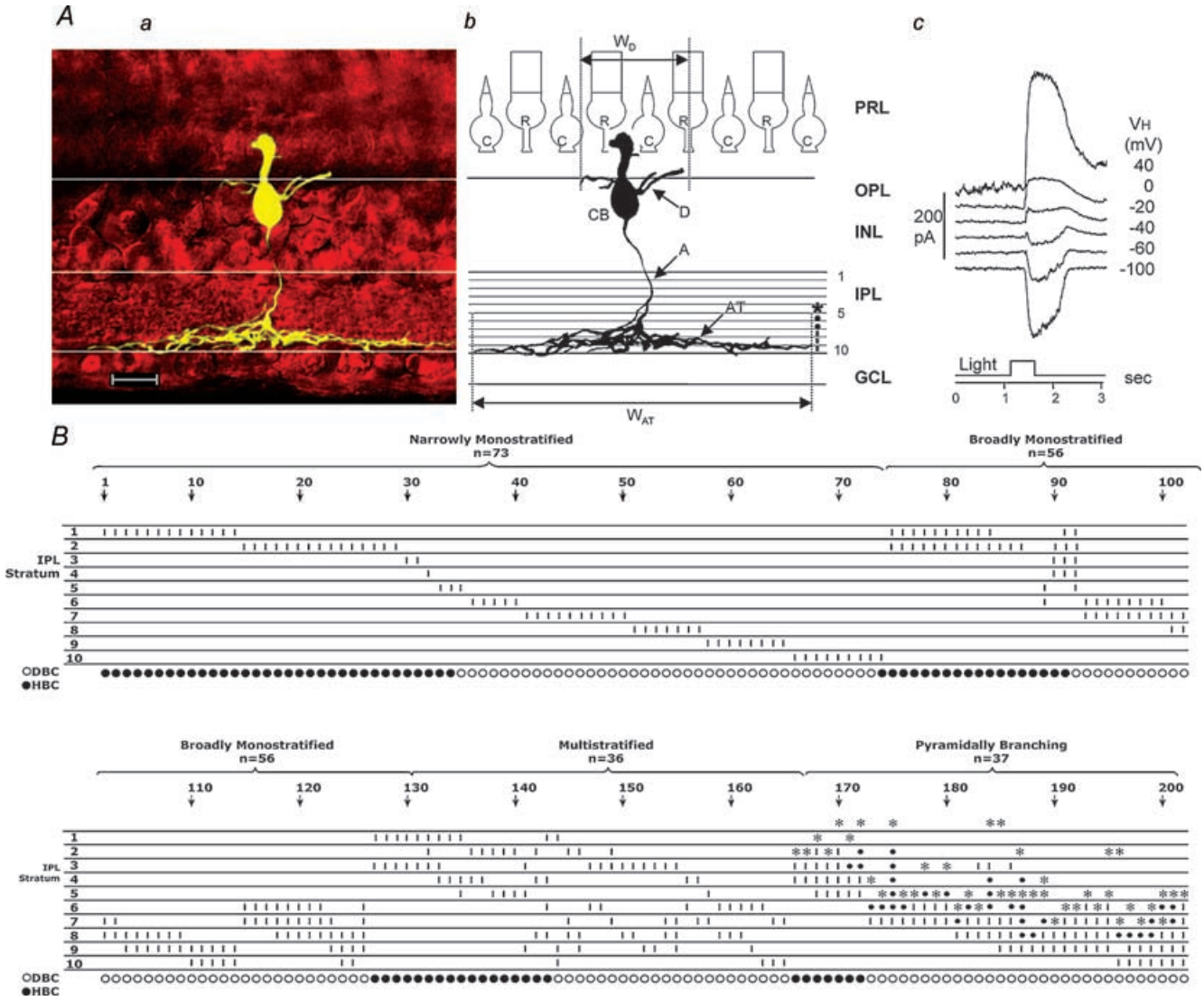

Figure 1. Distribution of axon terminal stratification patterns of bipolar cells

A, stacked confocal fluorescence image of a bipolar cell (*a*), sketch of the same cell on a schematic background of the retina with marked divisions of 10 strata of the IPL (*b*), and the light-evoked current responses to a 0.5-s light step (500 nm, –3.3 (3.3 log unit attenuation)) at various holding potentials (*c*). CB: cell body; D: dendrites; W_D: dendritic field width; W_{AT}: width of axon terminal; R: rod; C: cone; PRL: photoreceptor layer; OPL: outer plexiform layer; INL: inner nuclear layer; IPL: inner plexiform layer; GCL: ganglion cell layer; calibration bar: 25 μm. *B*, distribution of axon terminal stratification strata (1–10) in the IPL of 202 bipolar cells. These cells are grouped as 'narrowly monostratified', 'broadly monostratified', 'bistratified and multistratified' and 'pyramidally branching'. Each vertical column represents a bipolar cell (cell number is given every 10 cells above the arrows) and the short vertical bars in individual strata indicate the presence of axonal processes ramified in that stratum. *: initial branching point; small dot: branch passage. Bottom row: ○: ΔI_C is inward (ON cell or DBC); ●: ΔI_C is outward (OFF cell or HBC).

Photoreceptor inputs (ΔI_C)

At −60 mV, cells 1–5 exhibited sustained outward ΔI_C (and thus they are HBCs), and cells 6–10 gave rise to sustained inward ΔI_C (so they are DBCs). The outward ΔI_C in cells 1 and 2 was maintained for 1–2 s after light cessation, whereas a transient inward current that overshot below the ΔI_C baseline was observed at light cessation in cells 3–5 (the amplitude of the transient OFF overshoot was progressively larger as the cell's axon ramified closer to the centre of the IPL, cell 3→4→5). The inward ΔI_C in cells 6–9 were sustained during the light step and returned to the baseline with a small overshoot at light offset. The inward ΔI_C in cell 10, on the other hand, was maintained for 1–2 s after light cessation. These patterns of excitatory light responses were consistent in all narrowly monostratified bipolar cells within a given stratum (Fig. 1*B*), irrespective of their dendritic or axon terminal width. The mean (± S.D.) peak amplitudes of ΔI_C in various types of narrowly monostratified bipolar cells are given in the upper portion of Table 1. Since the equilibrium potential of the ΔI_C is near 0 mV (Maple *et al.* 1994), outward ΔI_C at −60 mV is accompanied by a conductance decrease whereas inward ΔI_C at −60 mV is accompanied by a conductance increase. Therefore, the excitatory inputs to strata 1–5 are likely to be mediated by the sign-preserving AMPA/kainate glutamate receptors (Slaughter & Miller, 1983; Maple *et al.* 1999), and those to strata 6–10 are likely be mediated by the sign-inverting L-AP4 glutamate receptors (Slaughter & Miller, 1981; Nawy & Jahr, 1990).

We also determined the relative rod/cone inputs of the ΔI_C in narrowly monostratified bipolar cells given in Figs 1*B* and 2 by using the spectral difference method described in earlier studies (Yang & Wu, 1990; Wu *et al.* 2000). In the tiger salamander retina, spectral difference, ΔS, defined as $S_{700} - S_{500}$ (where S_{700} and S_{500} are intensities (in log units) of 700 nm and 500 nm light eliciting responses of the same amplitude) for the rods is about 3.4 and that for the cones is about 0.1 (Yang & Wu, 1990), and thus bipolar cells with ΔS closer to 3.4 are more rod-dominated and those with ΔS closer to 0.1 are more cone-dominated. Figure 3 shows examples of how ΔS of a rod-dominated DBC (3*A*) and a cone-dominated DBC (3*B*) was determined. The mean (± S.D.) ΔS values of narrowly monostratified bipolar cells are also listed in the upper portion of Table 1. Cells in strata 1, 2 and 10 are the most rod-dominated bipolar cells with average $\Delta S > 2.5$, cells in stratum 3 are slightly less rod-dominated with an average ΔS of 2.2, cells in strata 4–8 are cone-dominated with an average $\Delta S < 1.0$, and cells in stratum 9 are less cone-dominated with an average ΔS of 1.5. These results correlate very well with the waveform of ΔI_C described above: ΔI_C of rod-dominated bipolar cells (cells 1, 2 and 10) returned to the baseline 1–2 s after light offset (similar to the slow response recovery of the rods (Wu, 1987*a*)), and ΔI_C of cone-dominated bipolar cells (cells 4–8)

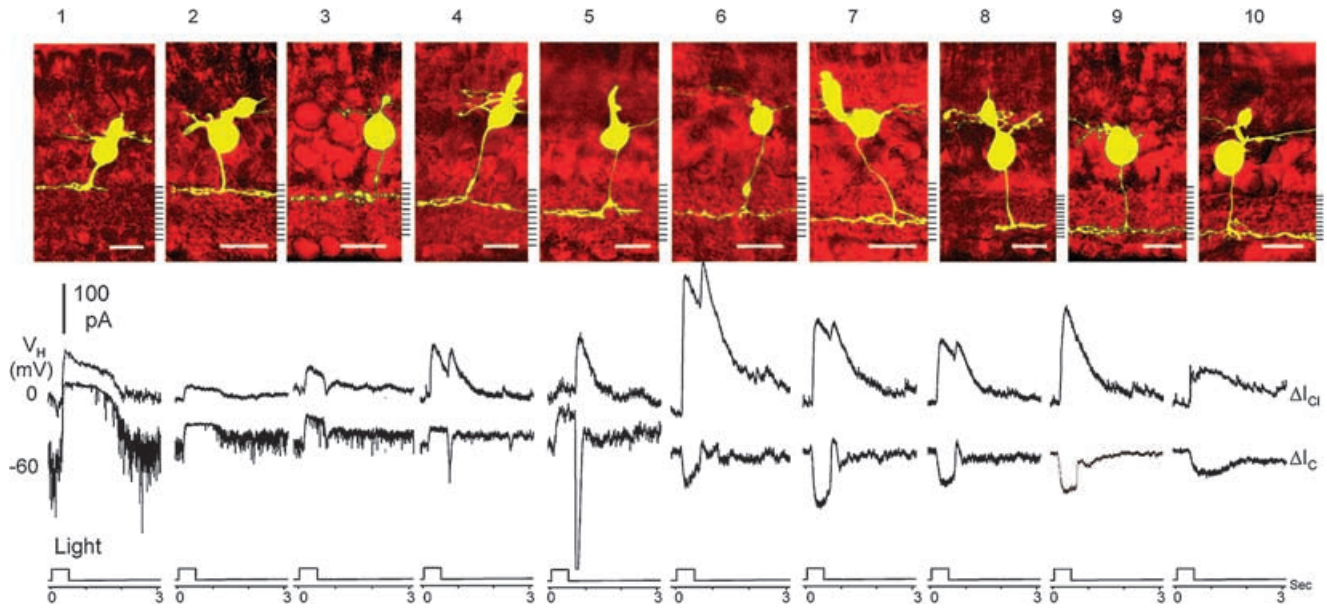

Figure 2
Top, stacked confocal fluorescent images of 10 (cells 1–10, corresponding to the stratum each cell ramifies) narrowly monostratified bipolar cells. Bottom, current responses evoked by a 0.5-s light step (500 nm, −3.3) at holding potentials near E_{Cl} (ΔI_C) and near E_C (ΔI_{Cl}).

Table 1. Light response attributes of narrowly monostratified bipolar cells (upper table) and broadly monostratified, multistratified and pyramidally branching bipolar cells listed in Fig. 4 (lower table)

Cell no.	1	2	3	4	5	6	7	8	9	10
Stratum	1	2	3	4	5	6	7	8	9	10
DBC/HBC	HBC	HBC	HBC	HBC	HBC	DBC	DBC	DBC	DBC	DBC
ΔI_C	ON^+	ON^+	ON^+	ON^+/OFF^-	ON^+/OFF^-	ON^-	ON^-	ON^-	ON^-	ON^-
ΔI_{Cl}	ON^+	ON^+	ON^+	ON^+/OFF^+	ON^+/OFF^+	ON^+/OFF^+	ON^+/OFF^+	ON^+/OFF^+	ON^+	ON^+
ΔS	2.9 ± 4 (7)	2.6 ± 5 (10)	2.2 ± 4 (2)	0.9 (1)	0.7 ± 0.2 (3)	0.9 ± 0.4 (5)	0.8 ± 0.3 (8)	0.6 ± 0.3 (7)	1.5 ± 0.6 (6)	2.5 ± 0.4 (8)
sEPSC (I_1)	44 ± 11 (7)	32 ± 9 (10)	23 ± 7 (2)	9 (1)	6 ± 2.2 (3)	–	–	–	–	–

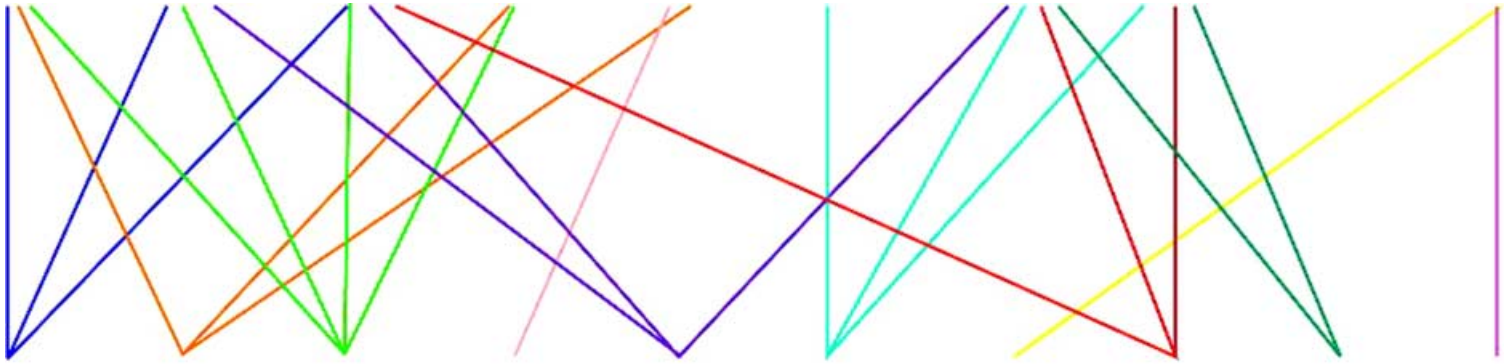

Cell no.	11	12	13	14	15	16	17	18	19	20
Stratum	1 + 2 + 3	1, 4 + 5	1 + 2 + 3 + 4	(1) 5	2 + 3, 7	6 + 7 + 8	(6) 10	3, 7 + 8	(0) 3, 7 + 8	(2) 10
DBC/HBC	HBC	HBC	HBC	HBC	DBC	DBC	DBC	DBC	DBC	DBC
ΔI_C	ON^+	ON^+/OFF^-	ON^+/OFF^-	ON^+/OFF^-	ON^+	ON^-	ON^-	ON^-	ON^-	ON^-
ΔI_{Cl}	ON^+	ON^+/OFF^+	ON^+/OFF^+	ON^+/OFF^+	ON^+/OFF^+	ON^+/OFF^+	ON^+	ON^+/OFF^+	ON^+/OFF^+	ON^+
ΔS	2.7	1.0	2.0	0.8	1.1	0.6	2.4	0.7	0.8	2.3
sEPSC (I_1)	37	8	29	11	–	–	–	–	–	–

Top, levels of axon terminal stratification (strata 1–10) and light response attributes of narrowly monostratified bipolar cells. Data are derived from cells 1–73 in Fig. 1*B*. DBC: depolarizing bipolar cell; HBC: hyperpolarizing bipolar cell (outward ΔI_C); ΔI_C: light-evoked cation current; ΔI_{Cl}: light-evoked chloride current; ON: current response at light onset; OFF: current response at light offset; +: outward current; −: inward current; ΔS: average spectral difference (in log units, ± S.D., *n*: number of cells for the mean values); sEPSC, spontaneous excitatory postsynaptic current (in pA). Bottom, levels of axon terminal stratification and light response attributes of the 10 broadly monostratified, multistratified and pyramidally branching bipolar cells in Fig. 3 (cell 11–20). Strata of the broadly monostratified band are connected with the '+' sign (e.g. 1 + 2 + 3), strata of separate axon terminal bands in multistratified cell are separated by the '−', sign, and the strata for the branching point of pyramidally branching cells are placed in parentheses. Middle, colour-coded lines connecting the light response attributes of the narrowly monostratified cells and the broadly monostratified, multistratified and pyramidally branching cells. The DBC/HBC, ON/OFF, $\Delta I_C/\Delta I_{Cl}$, ΔS and sEPSC properties of the the broadly monostratified and multistratified cells are close to the average corresponding properties of the narrowly monostratified cells in the same strata, and the properties of the pyramidally branching cells are similar to the properties of the narrowly monostratified cells whose axon terminals stratified in the same stratum as the pyramidal axon terminal *endings*.

returned to the baseline promptly at light offset (similar to the fast response recovery of the cones (Wu, 1988)). ΔI_C of cell 3 and 9 (with intermediate rod/cone dominance) exhibited a mixed rod- and cone-dominated ΔI_C waveform.

The spontaneous excitatory postsynaptic currents (sEPSCs), which are responsible for the prominent current noise visible in the HBC ΔI_C records (Maple *et al.* 1994), are different in rod-dominated HBCs and cone-dominated HBCs. sEPSCs decreased in frequency during light stimulus, which can be attributed to the decrease of current noise during light stimulation. sEPSCs in cells 4 and 5 were smaller and of lower frequency than those in cells 1–3, suggesting that sEPSCs in rod-dominated HBC (HBC_Rs) are larger and of higher frequency than the cone-dominated HBCs (HBC_Cs). We estimated average single sEPSC amplitude (I_1) by the variance/mean current ratio (variance of the current fluctuation in darkness divided by the amplitude of the current difference between darkness and bright light), and the I_1 values of cells 1–5 are listed in the upper portion of Table 1. The vast majority of DBCs did not exhibit any sEPSCs, probably because their excitatory inputs are mediated by the metabotropic glutamate receptors which are too slow to mediate the fast vesicular events in the synapses (Nawy & Jahr, 1991). The only DBCs that occasionally exhibited sEPSCs were those with axon terminals ramifying in both sublamina A and B (cells 144–157 in Fig. 1*B*, see also Fig. 5*B* left panel).

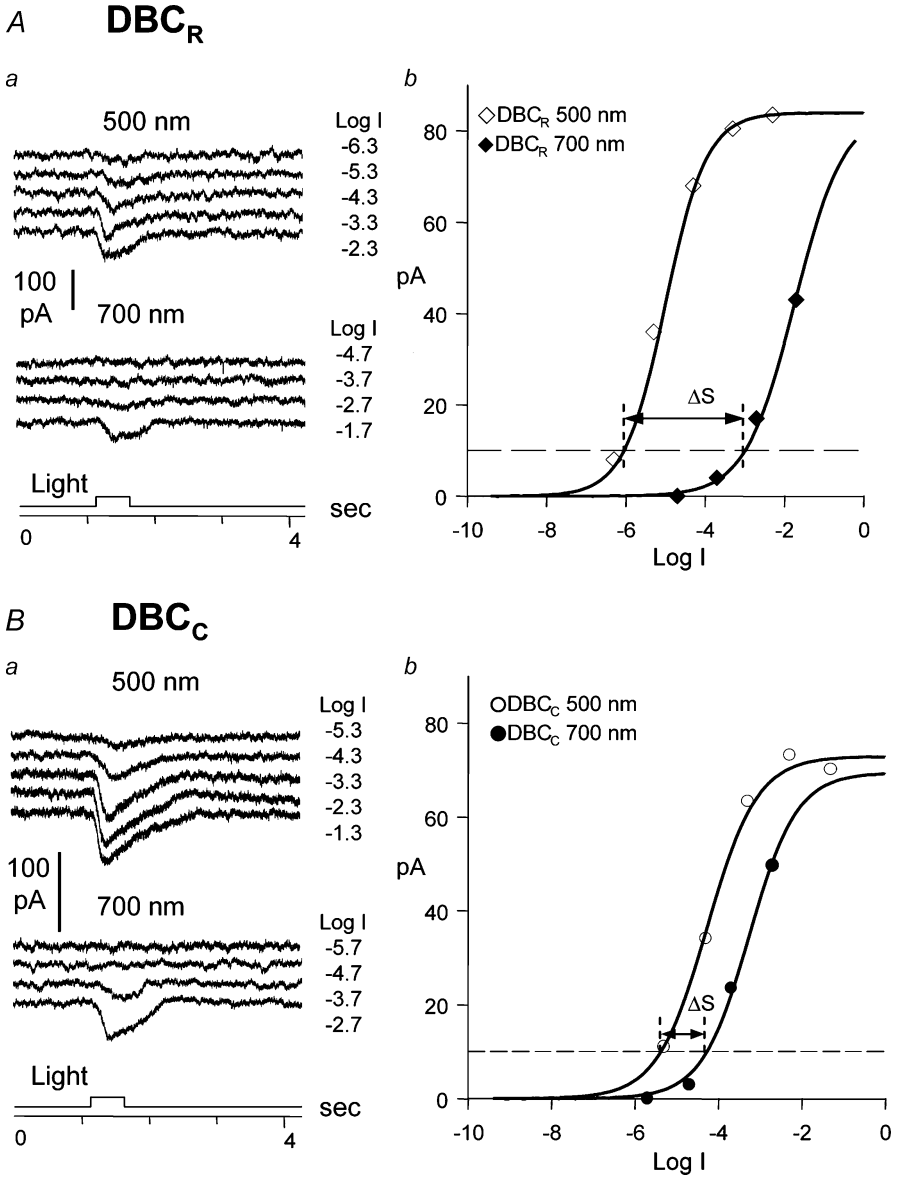

Figure 3
Aa and *Ba*, current responses of a rod-dominated DBC (DBC_R) (*A*) and a cone-dominated DBC (DBC_C) (*B*) to 500 nm and 700 nm light steps of various intensities (labelled in log unit of attenuation on the left of each current trace). *Ba* and *Bb*, the response–intensity relations of the current responses. For the criterion response of 10 pA marked by the horizontal dashed line, ΔS for the DBC_R is 3.1 log units and for the DBC_C is 0.8 log unit.

Amacrine cell inputs (ΔI_{Cl})

At 0 mV (near E_C), all bipolar cells, either DBCs or HBCs, exhibited outward ΔI_{Cl}, indicating that light-evoked inhibitory inputs in these cells were accompanied by a conductance increase (as E_{Cl} was near −60 mV). This suggests that all interneurones that release inhibitory neurotransmitters that gate ΔI_{Cl} in bipolar cells are depolarized by light. There is an ON/OFF rule for ΔI_{Cl} in narrowly monostratified bipolar cells. Cells 1, 2, 3, 9 and 10 exhibited ON ΔI_{Cl}, and cells 4–8 gave rise to ON–OFF ΔI_{Cl}. Similar to the waveform and sEPSCs of ΔI_C, this ΔI_{Cl} ON/OFF rule correlates with the cells' rod/cone dominance very well: ΔI_{Cl} of cone-dominated bipolar cells (cells 4–8) received light-evoked inhibitory inputs from ON–OFF interneurones, and ΔI_{Cl} of cells with more rod dominance (cells 1–3 and 9–10) received light-evoked inhibitory inputs from ON interneurones.

Stratum-by-stratum rules of narrowly monostratified cells are the basic building blocks for light responses of broadly monostratified, multistratified and pyramidally branching bipolar cells

Results in Fig. 2 and Table 1 (upper portion) suggest that various attributes of ΔI_C and ΔI_{Cl} of the narrowly monostratified bipolar cells correlate closely with the level of axon terminal stratification in the IPL. We next examined whether rules correlating patterns of axon terminal stratification and light response characteristics could be established for the broadly monostratified, multistratified and pyramidally branching bipolar cells. Figure 4 shows the morphology (upper panel), ΔI_{Cl} and ΔI_C (lower panel) of 10 (cells 11–20) bipolar cells. Cell 11 was broadly monostratified in strata 1 + 2 + 3, cell 12 was bistratified in strata 1 and 4 + 5, cell 13 was broadly monostratified in strata 1 + 2 + 3 + 4, and cell 14 had a pyramidally branching axon with a branching point in stratum 1 and terminal endings in stratum 5. These four cells had outward ΔI_C and thus they were HBCs. ΔI_C of cell 11 was sustained with slow recovery, whereas that of cells 12–14 had a sustained component and an OFF transient inward component. ΔI_{Cl} in cell 11 was sustained ON whereas that of cells 12–14 was transient ON–OFF. sEPSCs in cells 11 and 13 were of higher frequency and amplitude that those in cells 12 and 14. Cell 15 was bistratified in strata 2 + 3 and 7, cell 16 was broadly monostratified in strata 6 + 7 + 8, and cell 17 had a pyramidally branching axon with a branching point in stratum 6 and terminal endings in stratum 10. Cell 18 is bistratified in strata 3 and 7 + 8, cell 19 had a pyramidally branching axon with a branching point in the proximal portion of the INL and terminal endings in stratum 7 + 8 and a branch in stratum 3, and cell 20 had a pyramidally branching

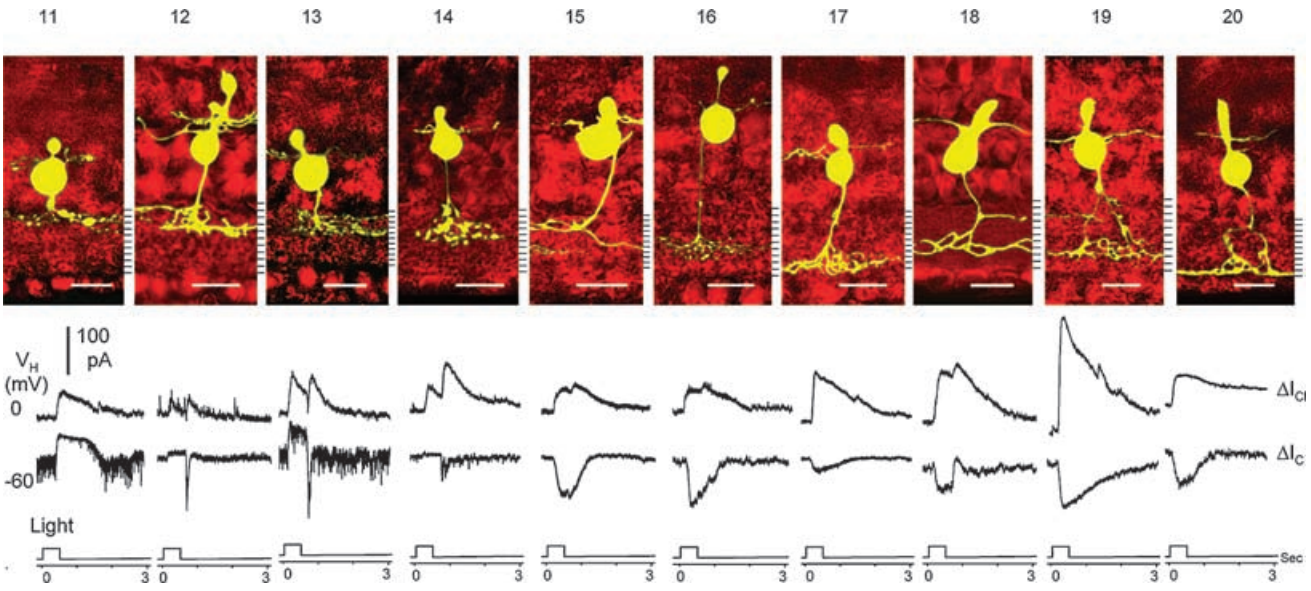

Figure 4
Top, stacked confocal fluorescent images of 10 (cells 11–20) broadly monostratified (cells 11, 13 and 16), multistratified (cells 12, 15 and 18), and pryamidally branching (cells 14, 17, 19 and 20) bipolar cells. Bottom, current responses evoked by a 0.5-s light step (500 nm, −3.3) at holding potentials near E_{Cl} (ΔI_C) and near E_C (ΔI_{Cl}).

axon with a branching point in stratum 2 and terminal endings in stratum 10. ΔI_C of these six cells were sustained inward currents and thus they were DBCs. ΔI_{Cl} of cells 17 and 20 were sustained ON, and those of cells 15–16 and 18–19 were ON–OFF. The ΔS values and average sEPSC amplitude of each of these 10 cells were measured and they are listed in the lower portion of Table 1.

The results in Figs 2 and 4 and Table 1 clearly suggest that the rules correlating DBC/HBC, ON/OFF responses, rod/cone dominance, sEPSC frequency/amplitude (for HBCs) and axon terminal stratification in the IPL set forth by narrowly monostratified cells are closely followed by broadly monostratified, multistratified and pyramidally branching bipolar cells: ΔI_C and ΔI_{Cl} of bipolar cells with axon terminals stratified in multiple strata exhibited combined $\Delta I_C/\Delta I_{Cl}$ properties of the narrowly monostratified cells in the same strata, and ΔI_C and ΔI_{Cl} of bipolar cells with pyramidally branching axons are very similar to the ΔI_C and ΔI_{Cl} of narrowly monostratified cells whose axon terminals stratified in the same stratum as the axon terminal *endings* of the pyramidally branching cell. It is also evident that the relative rod/cone inputs (as indicated by the ΔS values) to these cells are consistent with the rules set forth by the narrowly monostratified bipolar cells: bipolar cells with axon terminals stratified near the two margins of the IPL (strata 1, 2 and 10, and to a lesser degree strata 3 and 9) are more rod-dominated and those having axon terminals ramifying at the centre levels are more cone-dominated. Additionally, HBCs with axon terminals in strata 1–3 exhibit sEPSCs with a higher frequency and a larger amplitude. Furthermore, ΔI_{Cl} in cells with axon terminals predominantly in the rod strata (strata 1–3 and 9–10) (cells 11, 17 and 20) were ON, and cells with axon terminals predominantly in the cone strata (strata 4–8) (cells 12–16 and 17–19) were ON–OFF. These observations suggest that attributes of photoreceptor and amacrine cell inputs (ΔI_C and ΔI_{Cl}) in broadly monostratified, multistratified and pyramidally branching bipolar cells correlate closely with the levels (or strata) of their axon terminal stratification in the IPL: DBC/HBC, ON/OFF, rod/cone-dominance, and sEPSCs are projected to the IPL in a stratum-by-stratum fashion, and cells with multiple ΔI_C attributes project signals to multiple IPL strata as if they sum up ΔI_C of multiple narrowly monostratified cells with axon terminals in the corresponding strata. Therefore the 10 IPL strata are the basic building blocks for bipolar cell light response attributes and axon morphology. This is illustrated by the coloured lines connecting the upper and lower portions of Table 1: each colour represents a cell (cells 11–20) which shared the same axon terminal strata and light response properties of the narrowly monostratified cells.

DBCs and HBCs with axon terminals ramifying in both sublamina A and B are hybrid bipolar cells

The only apparent exceptions to the stratum-by-stratum rule are the multistratified bipolar cells with axon terminals ramified in both sublamina A and B. These cells account for about 10% of the total bipolar cells we recorded from the tiger salamander retina (cells 141–158, 181, 182 and 184, 21 out of a total of 202 cells in Fig. 1*D*). About 86% of these cells are DBCs (with inward ΔI_C, and we named them DBC_{AB}), 72% of which have their sublamina A axon in stratum 3 (cells 147–156, 181, 182 and 184, also see cells 15, 18 and 19 in Fig. 4). In regular DBCs (axons in sublamina B only), light-evoked current responses (ΔI_C and ΔI_{Cl}) are completely suppressed by 20 μM L-AP4, a metabotropic glutamate receptor agonist (Slaughter & Miller, 1981), as shown in Fig. 5*A*. In DBC_{AB}s, however, 20 μM L-AP4 converts the DBC responses into HBC responses: both ΔI_C and ΔI_{Cl} are outward, and these outward current responses were completely abolished by 100 μM GYKI (Fig. 5*B*), an AMPA receptor antagonist (Parsons *et al.* 1994; Sekiguchi *et al.* 1998). Additionally, some sEPSCs were occasionally observed in DBC_{AB}s (Fig. 5*B* left panel). These results suggest that DBC_{AB}s are hybrids of DBC/HBC, and their light responses are mediated by both L-AP4 and AMPA receptors although under dark-adapted conditions the L-AP4-mediated responses masked the AMPA-mediated responses.

We also recorded three HBCs whose axon terminals ramified in both sublamina A and B (cells 141–143 in Fig. 1*D*, we named them as HBC_{AB}s). Contrary to the regular HBCs in which light-evoked current responses (ΔI_C and ΔI_{Cl}) were completely suppressed by 100 μM GYKI (as shown in Fig. 6*A*), light-evoked current responses in HBC_{AB}s in GYKI became DBC-like: ΔI_C was inward and ΔI_{Cl} was outward (Fig. 6*B* middle panel), and these current responses were completely abolished by 20 μM L-AP4 (Fig. 6*B* right panel; ΔI_{Cl} was not suppressed in GYKI possibly because light responses of a subpopulation of salamander amacrine cells are mediated by kainate-preferring receptors and thus they are resistant to GYKI (J.-J. Pang and S. M. Wu, unpublished results)). These data suggest that HBC_{AB}s are also hybrids of DBC/HBC, and their light responses are mediated by both L-AP4 and AMPA receptors although under dark-adapted conditions the AMPA-mediated responses masked the L-AP4-mediated responses.

Discussion

Stratum-by-stratum analysis of bipolar cell morphology and function

We describe in this report a systematic examination of light response characteristics and axonal morphology of over 200 bipolar cells in dark-adapted tiger salamander retinal slices. This study differs from our previous report (Wu *et al.* 2000) in at least three ways. First, we used the confocal microscope (instead of the regular modulation contrast microscope) to reveal the detailed three-dimensional morphology of every recorded cell. This allowed us to generate a stratum-by-stratum map of the precise axon terminal stratification patterns of the bipolar cells. Secondly, we used the Nitemare binocular scopes for dissection and recording under infrared (instead of red light). This permits light response recordings from completely dark-adapted retinal slices and a more definitive separation of the rod- and cone-dominated signals. Thirdly, we extended the bipolar cell sample size by almost threefold. Consequently, we found a wide variety of morphological types of bipolar cells, and they fall into four major groups according to the patterns of axon terminal ramification in the IPL: 36% were narrowly monostratified, 27% were broadly monostratified, 19% were multistratified, and 18% bore pyramidally branching axons. This list of cells includes the 12 types of bipolar cells reported previously, but goes far beyond. For example, there were only five types of narrowly monostratified cells in strata 1, 2, 7, 9 and 10 in the previous report (Wu *et al.* 2000). Here we show narrowly monostratified cells in all 10 strata (Fig. 1*B*), though there are fewer cells with axons ramifying in the previously missing strata. This complete list of narrowly monostratified cells allows us to identify stratum-by-stratum rules for light response characteristics of bipolar cells. We also show in the present study more varieties of bistratified, multistratified and pyramidally branching cells, which permits us to determine the general

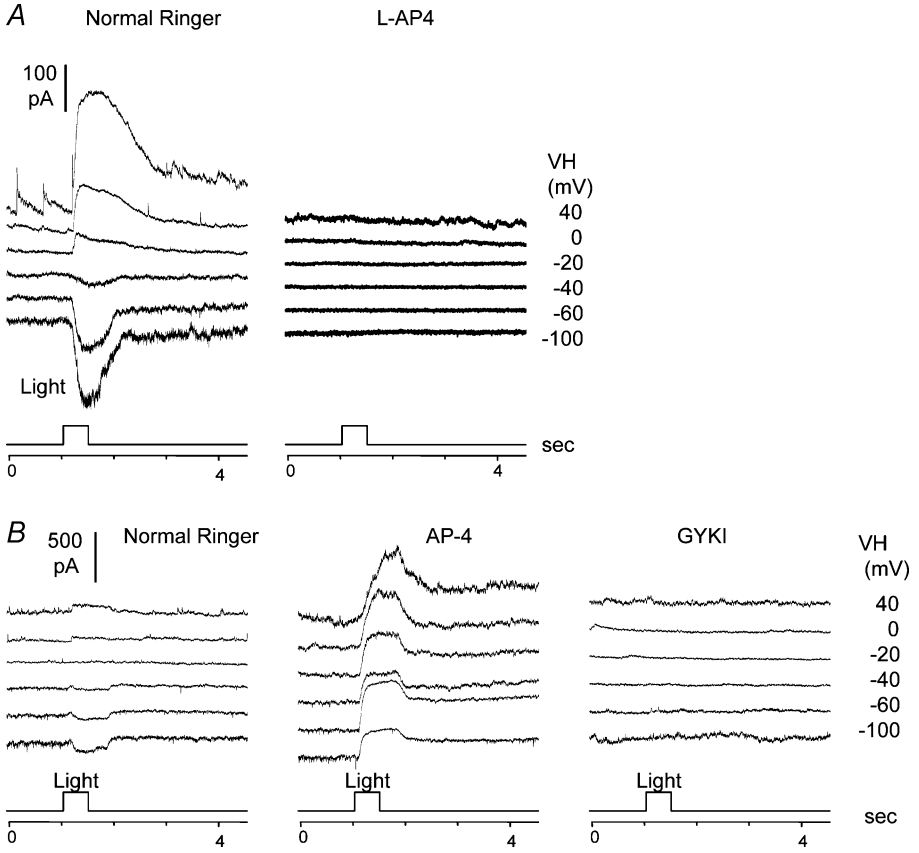

Figure 5

A, light-evoked current responses at various holding potentials (V_H) of a regular DBC (axons in sublamina B only, cell 108 in Fig. 1*B*) in normal Ringer solution (left panel) and in the presence of 20 μM L-AP4 (right panel). *B*, light-evoked current responses at various holding potentials (V_H) of a hybrid DBC (DBC_{AB}, axons in both sublamina A and B, cell 155 in Fig. 1*B*) in normal Ringer solution (left panel), in the presence of 20 μM L-AP4 (middle panel), and in the presence of 20 μM L-AP4 + 100 μM GYKI (right panel).

rules for correlating light response characteristics with axon terminal morphology for all bipolar cells.

General rules for bipolar cell light responses and axonal morphology

The stratum-by-stratum analysis of light response characteristics on narrowly monostratified cells (upper portion of Table 1), broadly monostratified, multistratified, and pyramidally branching bipolar cells (lower portion of Table 1) suggests that the 10 IPL strata are the basic building blocks for light response attributes and axonal morphology of all bipolar cells in the salamander retina. Additionally, we showed that bipolar cells with axons in both sublamina A and B are DBC–HBC hybrids, because their light responses are mediated by both L-AP4 and AMPA receptors. Based on these analyses, we propose several general rules that describe the function–morphology relationships of retinal bipolar cells. (1) Cells with axon terminals in strata 1–5 (sublamina A) are HBCs and those in strata 6–10 (sublamina B) are DBCs. This agrees with the sublamina A/B rule observed in many vertebrate species (Famiglietti *et al.* 1977; Nelson *et al.* 1978; Euler & Masland, 2000). (2) Cells with axon terminals ramifying in both sublaminae are DBC–HBC hybrids, as they express both L-AP4 and AMPA receptors. Most (over 85%) of these cells are DBCs (DBC_{AB}) under normal dark-adapted conditions, the majority of which have their sublamina A process in stratum 3. This may explain a curious previous finding in which the narrowly monostratified amacrine cells in stratum 3 (an OFF stratum) exhibit ON bipolar cell inputs (Pang *et al.* 2002*b*). Only about 14% of the hybrid bipolar cells are HBCs (HBC_{AB}) under normal dark-adapted conditions. (3) Cells with axon terminals in strata 1, 2 and 10 are rod-dominated, those in strata 4–8 are cone-dominated, and those in strata 3 and 9 exhibit intermediate rod/cone dominance. (4) HBCs exhibit sEPSCs but DBCs do not, except for the DBC_{AB}s, which exhibit some sEPSCs. A possible reason for the lack of sEPSCs in DBCs is that the metabotropic L-AP4 receptors may be too slow to mediate the fast sEPSC events (Dixon & Copenhagen, 1997). sEPSCs in rod-dominated HBCs are of larger amplitude and higher frequency than those of the cone-dominated HBCs, probably reflecting that the AMPA receptor kinetics of these two populations of cells

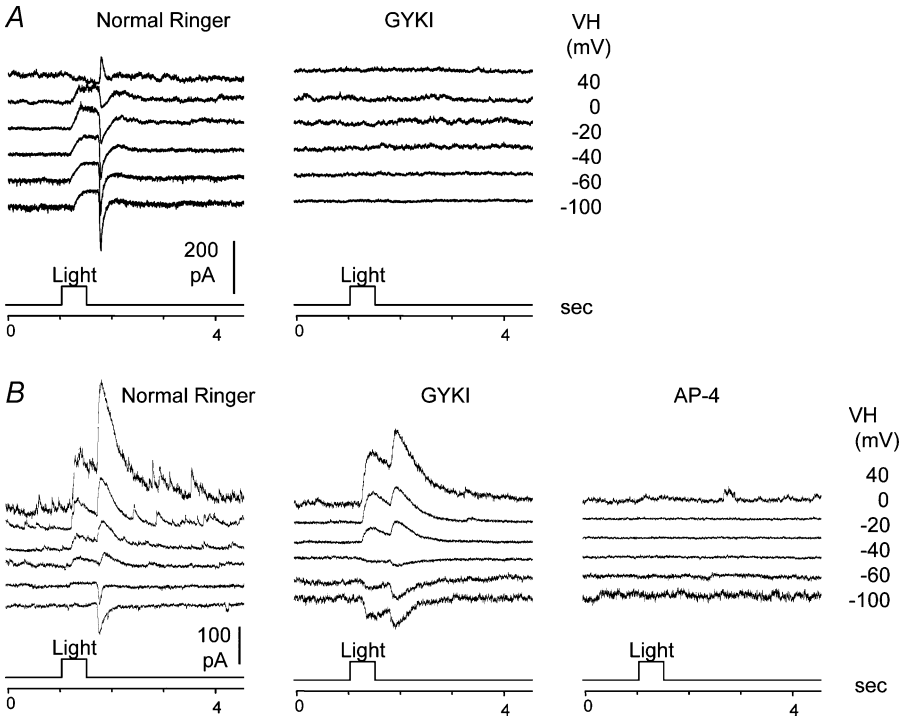

Figure 6

A, light-evoked current responses at various holding potentials (V_H) of a regular HBC (axons in sublamina A only, cell 35 in Fig. 1*B*) in normal Ringer solution (left panel) and in the presence of 100 μM GYKI (right panel). *B*, light-evoked current responses at various holding potentials (V_H) of a hybrid HBC (HBC_{AB}, axons in both sublamina A and B, cell 142 in Fig. 1*B*) in normal Ringer solution (left panel), in the presence of 100 μM GYKI (middle panel), and in the presence of 20 μM L-AP4 + 100 μM GYKI (right panel).

are different (Maple *et al.* 1999). (5) Light-evoked ΔI_C at light onset in rod-dominated HBCs are sustained and those of the cone-dominated HBCs exhibited a smaller sustained outward current followed by a transient inward current at the light offset. We did not, however, observe a clear transient/sustained dichotomy in DBCs reported by Awatramani & Slaughter (2000). For example, we never recorded any DBCs (whose identity was confirmed morphologically by Lucifer yellow fluorescence) that exhibited a transient inward ΔI_C at light onset with a decay time constant shorter than 400 ms). Although ΔI_C in different DBCs have different decay constants, we were unable to identify a pattern that correlated response kinetics and levels of axonal stratification in the IPL. (6) Interneurones mediating ΔI_{Cl} in rod-dominated bipolar cells exhibit ON light responses and those in cone-dominated bipolar cells exhibit ON–OFF light responses. We believe that ΔI_{Cl} in salamander bipolar cells are mainly mediated by amacrine cells because large portions of chloride conductance changes were induced by GABA/glycine application in the IPL (Wu & Maple, 1998) (although in some bipolar cells ΔI_{Cl} can be induced by glycine application in the OPL, presumably through interplexiform cell synapses (Maple & Wu, 1998)). This agrees with the finding that most amacrine cells in the tiger salamander retina are ON–OFF or ON cells, and the majority of the ON–OFF cells bear dendrites ramifying near the central region (cone-dominated strata) of the IPL (Pang *et al.* 2002*b*). (7) Bipolar cells with axon terminals stratified in multiple strata exhibited *combined* light response properties of the narrowly monostratified cells in the same strata. (8) Bipolar cells with pyramidally branching axons exhibit light response properties very similar to the responses of narrowly monostratified cells whose axon terminals stratified in the same stratum as the axon terminal *endings* of the pyramidally branching cell.

It is worth noting that the rules described here do not include all light response attributes, but only those attributes that correlate with the vertical distribution of bipolar cell axon terminals in the IPL. We did not describe, for example, the horizontal width of bipolar cell dendrites and axon terminals, which probably correlate with the receptive field size of bipolar cells and the third-order cells. This and other morphological features and their corresponding light response attributes of retinal bipolar cells will be described in future studies.

Are the rules derived from salamander bipolar cells applicable to other vertebrate species?

We believe that the rules derived from the salamander bipolar cells are, to a large extent, applicable to bipolar cells of other vertebrate species. Although technical difficulties, such as small soma size (which hinders physiological recordings) and short cell survival time in living slices (which limits the chance for obtaining good light responses), may have prohibited similar large-scale studies on bipolar cell function–morphology relationships in other species, evidence from mammals and several other animals has shown some remarkable agreements. For example, it has been demonstrated in many vertebrate species that HBCs have axons ramifying in the distal half (strata 1–5, sublamina A) of the IPL whereas DBCs send axons ramifying in the proximal half (strata 6–10, sublamina B) of the IPL (Famiglietti. & Kolb, 1976; Famiglietti *et al.* 1977; Euler & Masland, 2000). Additionally, anatomical evidence has shown that axon terminals of mammalian rod depolarizing bipolar cells end at the proximal edge (equivalent to stratum 10) of the IPL (Boycott & Wassle, 1991; Wassle *et al.* 1991), whereas the majority of the cone bipolar cells bear axons that ramify in the central strata of the IPL (Euler & Wassle, 1995; Hartveit, 1997). Although for many years anatomical studies were unable to identify rod HBCs in the mammalian retina, recent physiological and genetic evidence suggests that a rod OFF pathway must exist in mammals (Devries & Baylor, 1995; Soucy *et al.* 1998), perhaps with a non-conventional ultrastructure (Tsukamoto *et al.* 2001). Furthermore, recent studies have revealed that the rabbit retina contains more than a dozen types of ganglion cells, each with dendrites narrowly monostratified in one of the 10 strata of IPL and each carrying a unique set of excitatory and inhibitory inputs (Roska & Werblin, 2001; Roska & Werblin, 2003). These results suggest that, similar to the salamander bipolar cells, rabbit bipolar cells may project a unique set of excitatory synaptic signals to the ganglion cells in each of the 10 IPL strata.

Implications of stratum-by-stratum rules in retinal organization and development

The results described in this article suggest that bipolar cells project various light response attributes to segregated laminar regions (strata) of the IPL. Axons of narrowly monostratified bipolar cells form 10 parallel, stacked representations of input signals for the ganglion cell and amacrine cell dendrites. Broadly monostratified and multistratified bipolar cells sum light response attributes of multiple IPL strata and form broader bands of parallel representations. Narrowly monostratified amacrine cells and ganglion cells inherit light response attributes from narrowly monostratified bipolar cells in the same stratum (one-to-one) and multistratified

bipolar cells (strata convergence) (Roska & Werblin, 2001; Pang *et al.* 2002*b*). Multistratified amacrine cells and ganglion cells exhibit light response attributes from multiple narrowly monostratified bipolar cells (strata divergence) and multistratified bipolar cells (one-to-one, strata convergence or divergence) (Pang *et al.* 2002*a*). Similarly, the light-evoked inhibitory signals (ΔI_{Cl}) in a given bipolar cell share the same light response attributes of amacrine cells with dendrites in the same strata by the same set of computational algorithms (one-to-one, strata convergence and divergence).

The close correlation between bipolar cell light response attributes and patterns of axon terminal stratification suggest that synaptic inputs (which mediate bipolar cell light responses) must somehow influence the formation of synaptic outputs (levels of bipolar cell axon terminals in the IPL) during retinal development. It has been shown in several parts of the visual system that light-evoked neural activities facilitate laminar axonal projection and connectivity refinement by synaptic elimination (Shatz, 1990; Wong, 1999; Tavazoie & Reid, 2000). During retinal development, each bipolar cell light response attribute may promote axon projection in one or more strata by eliminating synapses in other strata of the IPL. Systematic developmental studies on retinal bipolar cells are needed to test this hypothesis.

References

Awatramani GB & Slaughter MM (2000). Origin of transient and sustained responses in ganglion cells of the retina. *J Neurosci* **20**, 7087–7095.

Boycott BB & Wassle H (1991). Morphological classification of bipolar cells of the primate retina. *Eur J Neurosci* **3**, 1069–1088.

Boycott B & Wassle H (1999). Parallel processing in the mammalian retina: the Proctor Lecture. *Invest Ophthalmol Vis Sci* **40**, 1313–1327.

Devries SH & Baylor DA (1995). An alternative pathway for signal flow from rod photoreceptors to ganglion cells in mammalian retina. *Proc Natl Acad Sci U S A* **92**, 10658–10662.

Dixon DB & Copenhagen DR (1997). Metabotropic glutamate receptor-mediated suppression of an inward rectifier current is linked via a cGMP cascade. *J Neurosci* **17**, 8945–8954.

Enroth-Cugell C & Robson JG (1966). The contrast sensitivity of retinal ganglion cells of the cat. *J Physiol* **187**, 517–552.

Euler T & Masland RH (2000). Light-evoked responses of bipolar cells in a mammalian retina. *J Neurophysiol* **83**, 1817–1829.

Euler T & Wassle H (1995). Immunocytochemical identification of cone bipolar cells in the rat retina. *J Comp Neurol* **361**, 461–478.

Famiglietti EV Jr, Kaneko A & Tachibana M (1977). Neuronal architecture of on and off pathways to ganglion cells in carp retina. *Science* **198**, 1267–1269.

Famiglietti EV Jr & Kolb H (1976). Structural basis for ON- and OFF-center responses in retinal ganglion cells. *Science* **194**, 193–195.

Field GD & Rieke F (2002). Mechanisms regulating variability of the single photon responses of mammalian rod photoreceptors. *Neuron* **35**, 733–747.

Hartveit E (1997). Functional organization of cone bipolar cells in the rat retina. *J Neurophysiol* **77**, 1716–1730.

Hubel DH & Livingstone MS (1987). Segregation of form, color, and stereopsis in primate area 18. *J Neurosci* **7**, 3378–3415.

Hubel DH & Wiesel TN (1977). Ferrier lecture. Functional architecture of macaque monkey visual cortex. *Proc R Soc Lond B Biol Sci* **198**, 1–59.

Katz B & Miledi R (1972). The statistical nature of the acetycholine potential and its molecular components. *J Physiol* **224**, 665–699.

Maple BR, Gao F & Wu SM (1999). Glutamate receptors differ in rod- and cone-dominated off-center bipolar cells. *Neuroreport* **10**, 3605–3610.

Maple BR, Werblin FS & Wu SM (1994). Miniature excitatory postsynaptic currents in bipolar cells of the tiger salamander retina. *Vision Res* **34**, 2357–2362.

Maple BR & Wu SM (1998). Glycinergic synaptic inputs to bipolar cells in the salamander retina. *J Physiol* **506**, 731–744.

Nawy S & Jahr CE (1990). Suppression by glutamate of cGMP-activated conductance in retinal bipolar cells. *Nature* **346**, 269–271.

Nawy S & Jahr CE (1991). cGMP-gated conductance in retinal bipolar cells is suppressed by the photoreceptor transmitter. *Neuron* **7**, 677–683.

Nelson R, Famiglietti EV Jr & Kolb H (1978). Intracellular staining reveals different levels of stratification for on- and off-center ganglion cells in cat retina. *J Neurophysiol* **41**, 472–483.

Pang JJ, Gao F & Wu SM (2002*a*). Relative contributions of bipolar cell and amacrine cell inputs to light responses of ON, OFF and ON-OFF retinal ganglion cells. *Vision Res* **42**, 19–27.

Pang JJ, Gao F & Wu SM (2002*b*). Segregation and integration of visual channels: layer-by-layer computation of ON-OFF signals by amacrine cell dendrites. *J Neurosci* **22**, 4693–4701.

Parsons CG, Gruner R & Rozental J (1994). Comparative patch clamp studies on the kinetics and selectivity of glutamate receptor antagonism by 2,3-dihydroxy-6-nitro-7-sulfamoyl-benzo(F)quinoxaline (NBQX) and 1-(4-amino-phenyl)-4-methyl-7,8-methyl-endioxyl-5H-2,3-benzodiaze pine (GYKI 52466). *Neuropharmacology* **33**, 589–604.

Roska B & Werblin F (2001). Vertical interactions across ten parallel, stacked representations in the mammalian retina. *Nature* **410**, 583–587.

Roska B & Werblin F (2003). Rapid global shifts in natural scenes block spiking in specific ganglion cell types. *Nat Neurosci* **6**, 600–608.

Sekiguchi M, Takeo J, Harada T, Morimoto T, Kudo Y, Yamashita S, Kohsaka S & Wada K (1998). Pharmacological detection of AMPA receptor heterogeneity by use of two allosteric potentiators in rat hippocampal cultures. *Br J Pharmacol* **123**, 1294–1303.

Shatz CJ (1990). Competitive interactions between retinal ganglion cells during prenatal development. *J Neurobiol* **21**, 197–211.

Slaughter MM & Miller RF (1981). 2-Amino-4-phosphonobutyric acid: a new pharmacological tool for retina research. *Science* **211**, 182–185.

Slaughter MM & Miller RF (1983). Bipolar cells in the mudpuppy retina use an excitatory amino acid neurotransmitter. *Nature* **303**, 537–538.

Soucy E, Wang Y, Nirenberg S, Nathans J & Meister M (1998). A novel signaling pathway from rod photoreceptors to ganglion cells in mammalian retina. *Neuron* **21**, 481–493.

Tavazoie SF & Reid RC (2000). Diverse receptive fields in the lateral geniculate nucleus during thalamocortical development. *Nat Neurosci* **3**, 608–616.

Thibos LN & Werblin FS (1978). The response properties of the steady antagonistic surround in the mudpuppy retina. *J Physiol* **278**, 79–99.

Tsukamoto Y, Morigiwa K, Ueda M & Sterling P (2001). Microcircuits for night vision in mouse retina. *J Neurosci* **21**, 8616–8623.

Wassle H, Yamashita M, Greferath U, Grunert U & Muller F (1991). The rod bipolar cell of the mammalian retina. *Vis Neurosci* **7**, 99–112.

Werblin FS (1978). Transmission along and between rods in the tiger salamander retina. *J Physiol* **280**, 449–470.

Wong RO (1999). Retinal waves and visual system development. *Annu Rev Neurosci* **22**, 29–47.

Wu SM (1987*a*). Light-dependent synaptic delay between photoreceptors and horizontal cells in the tiger salamander retina. *Vision Res* **27**, 363–367.

Wu SM (1987*b*). Synaptic connections between neurons in living slices of the larval tiger salamander retina. *J Neurosci Meth* **20**, 139–149.

Wu SM (1988). The off-overshoot responses of photoreceptors and horizontal cells in the light-adapted retinas of the tiger salamander. *Exp Eye Res* **47**, 261–268.

Wu SM, Gao F & Maple BR (2000). Functional architecture of synapses in the inner retina: segregation of visual signals by stratification of bipolar cell axon terminals. *J Neurosci* **20**, 4462–4470.

Wu SM & Maple BR (1998). Amino acid neurotransmitters in the retina: a functional overview. *Vision Res* **38**, 1371–1384.

Yang XL & Wu SM (1990). Synaptic inputs from rods and cones to horizontal cells in the tiger salamander retina. *Sci China B* **33**, 946–954.

Acknowledgements

We thank Dr Roy Jacoby and Ms Holly Vargo for critically reading this manuscript. This work was supported by grants from NIH (EY 04446), NIH Vision Core (EY 02520), the Retina Research Foundation (Houston), and Research to Prevent Blindness, Inc.